Proceedings of the 17th World Congress
The International Federation of Automatic Control
Seoul, Korea, July 6-11, 2008

A Vision-Based Technique for Vehicle Slip and Velocity Estimation

Xiaojing Song*, Lakmal D Seneviratne**
Kaspar Althoefer*, Zibin Song****, S. M. Vahed*****

** Department of Mechanical Engineering, King's College London, WC2R 2LS UK (e-mail:song.xiaojing@ kcl.ac.uk).*
, ***, *, ***** Department of Mechanical Engineering, King's College London, WC2R 2LS UK*

Abstract: This paper proposes a novel technique to estimate slips and velocities of an unmanned ground vehicle (UGV). A visual odometry sensor looking down the terrain surface is employed to measure the motion of the UGV, by tracking features selected from the terrain surface. The visual odometry sensor can provide motion information even when the terrain surface contains no distinctive features. A sliding mode observer (SMO) based-on a kinematic model is designed to deal with noise and uncertainty of the measurements from the visual odometry sensor, and simultaneously estimate the slip and velocity vectors of the UGV. The non-GPS slip and velocity estimation technique is independent of terrain parameters and robust to noise and uncertainty. Experimental results are given to show that the technique has good potential for vehicle slip and velocity estimation.

1. INTRODUCTION

Slip plays a vital role in an unmanned ground vehicle (UGV) traction control and stability control (Le 1999). Thus, accurate estimation of slip parameters, including linear slips and slip angle, are necessary for this purpose.

Slip parameter estimation requires vehicle velocity and wheel angular velocities. Wheel angular velocities can normally be acquired from optical wheel encoders. Many existing techniques used for position measurements can be applied to obtain vehicle velocity, which is the derivative of position with respect to time. A low-cost Inertial Navigation System (INS) together with an Extended Kalman Filter (EKF) is used for position estimation of a mobile robot in (Barshan *et al*., 1995); however, position provided by the INS is prone to cumulative errors. An optical encoder at the fifth wheel measures distance traveled by the vehicle, derivatives of which with respect to time give the vehicle velocities (Lee *et al*., 2004); however, the velocity errors are significant if the tracked vehicle moves over uneven ground. Global Positioning System (GPS)/Differential Global Positioning System (DGPS) is also widely used for position and velocity measurements. A civilian-based GPS is implemented for position measurements (Cooper *et al*., 1994). Despite integrating the GPS signal with inertial navigation information in an EKF, experimental results show that the position error still exists. GPS sometimes suffers from signal interference and signal loss, which may lead to inaccurate measurements of the position and velocity of the vehicle. Further, due to the low update frequency of GPS/DGPS, it can not be used as a stand-alone slip measurement system. Two Kalman Filters (KFs), a model based filter and a kinematic filter, integrating GPS with Inertial Measurement Unit (IMU) are used to give a high update rate of the vehicle states (Anderson *et al*., 2004); however, only slip angle is considered in this paper.

Visual odometry has become an attractive alternative for motion estimation in recent years. A CCD camera integrated with odometry for motion estimation is presented in (Nagatani *et al.*, 2000). An omnidirectional vision system is utilized to estimate the motion of an indoor mobile robot in (Bunschoten *et al.*, 2003). A television camera mounted parallel to the road surface is used to estimate the motion of the vehicle using optical flow information (Giachetti *et al*., 1998).

A novel vision-based technique combined with a sliding mode observer (SMO) to estimate slips and velocities of an UGV is proposed in this paper. An on-board monocular camera looking down at the terrain surface is employed as a visual odometry sensor to provide measurements of pose and velocity of the UGV. However, since measurements obtained form the visual odometry sensor are susceptible to noise and uncertainty, a SMO based-on a kinematic model of the UGV is designed to deal with the noise and uncertainty and give accurate estimated slip and velocity vectors of the UGV.

2. SYSTEM FLOWCHART

Fig. 1 shows the flowchart of the slip and velocity estimation system. The visual odometry sensor selects features from the terrain surface and tracks them in a sequence of images. The vehicle pose vector $[X, Y, \Phi]$ and vehicle longitudinal velocity $\dot{y}$ are derived using the motion decomposition method in the visual odometry sensor.

Since the measurements from visual odometry sensor are prone to noise and uncertainty when the UGV moves in real environments, the SMO based-on a kinematic model is designed for coping with noise and uncertainty and

estimating the slip and velocity vectors of the UGV. Two optical encoders attached to the driving wheels of the UGV provide angular velocity vector $[\omega_o, \omega_i]$. Receiving the angular velocity vector $[\omega_o, \omega_i]$, the vehicle pose vector $[X, Y, \Phi]$ and the vehicle longitudinal velocity $\dot{y}$, the SMO is driven to estimate the slip parameter vector $[i_o, i_i, \alpha]$ and the velocity vector $[\dot{\hat{x}}, \dot{\hat{y}}, \dot{\hat{\phi}}]$.

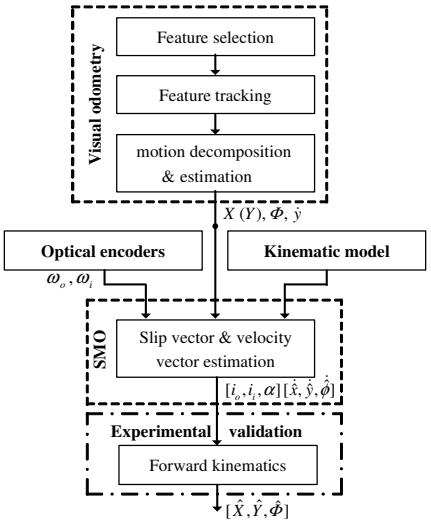

Fig. 1. Slip and velocity estimation algorithm framework

For validating the slip and velocity estimation technique, the forward kinematics of the vehicle is used to calculate the pose vector $[\hat{X}, \hat{Y}, \hat{\Phi}]$, using the estimated vehicle slip vector $[i_o, i_i, \alpha]$ from the SMO. If the estimated trajectory $[\hat{X}(t), \hat{Y}(t), \hat{\Phi}(t)]$ has good agreement with the real one, the slip vector and velocity vector estimated by the technique are validated to be accurate.

3. VISUAL ODOMETRY FOR MOTION MEASUREMENTS

In this study, since the camera is rigidly mounted on the UGV facing down the terrain surface, the motion of the UGV can be derived from the camera motion. The linear motion measurements in (Song X. *et al.*, 2007) are extended to 2-D in this paper.

3.1 Camera Model

A pinhole camera model, as shown in Fig. 2, is used to find the geometrical relationship between a small feature window on the terrain surface and its corresponding window on the image plane. To simplify, a normalized image plane is placed between the focal point of the camera and an object.

Let $P(X_R, Y_R, Z_R)$ be the central point of a small feature window on the terrain surface. This window is projected onto the normalized image plane (with the focal length being 1) perpendicular to the optical axis (Z axis). Let the corresponding window on the image plane be $P'(x_p, y_p, z_p)$. Z_R is the distance from the projection centre of the camera to the point $R(0,0,Z_R)$, which is the projection point from P to the optical axis. The

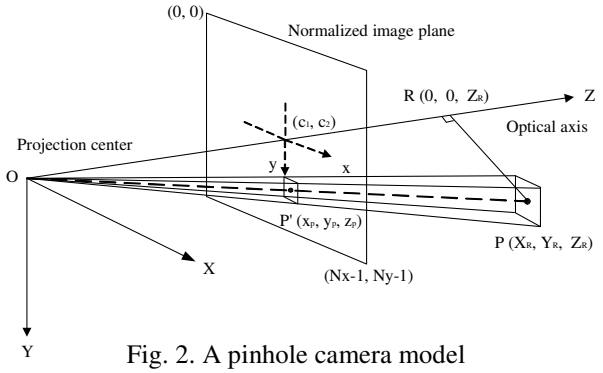

Fig. 2. A pinhole camera model

location of the projection point P' on the image plane is given by

$$\begin{bmatrix} x_p \\ y_p \end{bmatrix} = \begin{bmatrix} f_1(x_d + \alpha_c y_d) + c_1 \\ f_2 y_d + c_2 \end{bmatrix} \tag{1}$$

where

$$\begin{bmatrix} x_d \\ y_d \end{bmatrix} = (1 + k_1 r^2 + k_2 r^4 + k_5 r^6) \begin{bmatrix} x_n \\ y_n \end{bmatrix} + \begin{bmatrix} 2k_3 x_n y_n + k_4 (r^2 + 2x_n^2) \\ k_3 (r^2 + 2y_n^2) + 2k_4 x_n y_n \end{bmatrix} \tag{2}$$

where $r = \sqrt{x_n^2 + y_n^2}$. In (2), $[x_n, y_n]^T$ can be given by

$$\begin{bmatrix} x_n \\ y_n \end{bmatrix} = \begin{bmatrix} X_R / Z_R \\ Y_R / Z_R \end{bmatrix} \tag{3}$$

In (1) and (2), $k_n (n = 1, 2, \cdots, 5)$ represents distortion parameters of the camera, c_1, c_2 are the coordinates of the principal point of the image plane, α_c is the skew coefficient and f_1, f_2 are the focal lengths expressed in units of horizontal and vertical pixels. All these parameters can be obtained from camera calibration (Bouguet 2007).

3.2 Camera Velocity and Image Velocity

Based on the camera model, the camera motion can be obtained from the image velocity. For simplification, it is assumed that there is no distortion and skew coefficient of the camera. Thus, substituting $\alpha_c = 0$ and $k_n = 0 (n = 1, 2, \cdots, 5)$ into (1) and (2) gives

$$\begin{bmatrix} x_p \\ y_p \end{bmatrix} = \begin{bmatrix} f_1 X_R / Z_R + c_1 \\ f_2 Y_R / Z_R + c_2 \end{bmatrix} \tag{4}$$

Differentiating (4) with respect to time, the velocity of the camera is obtained by

$$\begin{bmatrix} \dot{X}_R \\ \dot{Y}_R \end{bmatrix} = \begin{bmatrix} (Z_R \dot{x}_p + (x_p - c_1)\dot{Z}_R) / f_1 \\ (Z_R \dot{y}_p + (y_p - c_2)\dot{Z}_R) / f_2 \end{bmatrix} \tag{5}$$

where $[\dot{X}_R, \dot{Y}_R]$ is the camera velocity vector and $[\dot{x}_p, \dot{y}_p]$ is the image velocity vector. Assuming that the terrain surface is predominantly flat, (5) can be further reduced to

$$\begin{bmatrix} \dot{X}_R \\ \dot{Y}_R \end{bmatrix} = \begin{bmatrix} Z_R \dot{x}_p / f_1 \\ Z_R \dot{y}_p / f_2 \end{bmatrix} \tag{6}$$

If the image velocity vector is known, the camera velocity can accordingly be obtained by (6).

Good feature windows are selected according to Shi-Tomasi detector (Shi *et al.*, 1994). The Lucas-Kanade image registration technique (Lucas *et al.*, 1981) and the Newton-Raphson method are employed in this study for tracking features. If feature windows are successfully tracked, the change of their locations on local image frames can be further used to calculate the instantaneous translation and rotation of the UGV.

In order to ensure any mistracked feature windows are rejected, two schemes are used: consistency check and statistical check. Let I_1 and I_2 be two consecutive images. Consistency check tracks features both from I_1 to I_2 and from I_2 to I_1. Statistical check wipes out those features which lead to large deviations from the median of measured pose and velocity (Milella *et al.*, 2006). After these two outlier discrimination checks, the remaining feature windows are finally chosen for calculating the pose and velocities of the UGV.

3.3 Motion Decomposition

The motion of the camera can be decoupled into a translational motion in a plane and a rotational motion about the optical axis. Let *Image 0* and *Image 1* be two consecutive images captured by the camera. P_0 is defined as a projected feature point on the image plane. Let the translation in horizontal and vertical directions be Δx and Δy respectively, and the rotational angle be θ.

The location of P_0 changes on the local image plane, after a movement of the camera within a short time interval. Let $(x_{P_0}^j, y_{P_0}^j)$ be the location of P_0 on *Image* j ($j = 0, 1$). The resultant motion of point P_0 can be expressed as

$$\begin{bmatrix} x_{P_0}^0 \\ y_{P_0}^0 \end{bmatrix} = \begin{bmatrix} x_{P_0}^1 \cos\theta - y_{P_0}^1 \sin\theta + \Delta x \\ x_{P_0}^1 \sin\theta + y_{P_0}^1 \cos\theta + \Delta y \end{bmatrix} = R \begin{bmatrix} x_{P_0}^1 \\ y_{P_0}^1 \end{bmatrix} + T \tag{7}$$

where, T is defined as a translation matrix and R is defined as a rotation matrix, then (7) is rewritten as

$$F = RS + T \tag{8}$$

where $F = [x_{p_0}^0, y_{p_0}^0]^T$ and $S = [x_{p_0}^1, y_{p_0}^1]^T$.

Actually, at least a pair of feature points is successfully tracked from one image to the next, then the unknown elements $(\Delta x, \Delta y, \theta)$ in matrices R and T can be obtained. In order to enhance the accuracy of calculated translation and rotation, normally hundreds of features are selected. A set of equations including the error items are given by

$$F_i = RS_i + T + E_i \tag{9}$$

To find matrices R and T, the aim is to minimize the weighted sum of squares. w_i are the weights in (10).

$$\sum_{i=1}^{n} w_i E_i^T E_i = \sum_{i=1}^{n} w_i (F_i - RS_i - T_i)^T (F_i - RS_i - T) \tag{10}$$

The rotation R makes the optimization nonlinear, thus, the method in (Schonemann, 1970) is used to compute R and T. This method applies Lagrange multipliers to force R to be orthogonal and takes the singular value decomposition of R.

Given the translation and rotation of the images, the camera motion can be easily derived using coordinates transformation. The pose $[X, Y, \Phi]$ and instantaneous velocity $[\dot{x}, \dot{y}, \dot{\phi}]$ of the UGV can be accordingly calculated.

4. SLIDING MODE OBSERVER FOR SLIP AND VELOCITY ESTIMATION

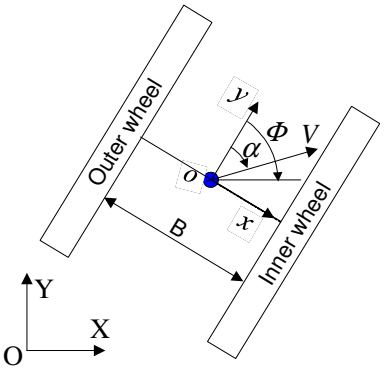

Fig. 3. Free body diagram of a skid-steered mobile robot

The UGV considered in this paper is a skid-steered mobile robot. Theoretically, the slip parameters of the skid-steered mobile robot in Fig. 3 are given by

$$\begin{aligned} i_o &= 1 - (\dot{y} + \dot{\Phi} \cdot \frac{B}{2}) / (\omega_o r) \\ i_i &= 1 - (\dot{y} - \dot{\Phi} \cdot \frac{B}{2}) / (\omega_i r) \\ \alpha &= \tan^{-1}(\dot{x} / \dot{y}) \end{aligned} \tag{11}$$

where i_o, i_i are the linear slips of outer and inner wheels and α is the slip angle of the vehicle, B is the tread of the vehicle, r is the effective radius of the wheel, ω_o, ω_i are the angular velocities of outer and inner wheels, $\dot{y}$ is the longitudinal velocity of the vehicle along y direction and $\dot{\Phi}$ is the yaw rate of the vehicle. $\dot{y}$ and $\dot{\Phi}$ measured by the visual odometry sensor, are prone to random noise and uncertainty. Thus, a sliding mode observer (SMO) based on a kinematic model of the skid-steered mobile robot is developed to cope with the noise and uncertainty, and estimate slip and velocity vectors of the vehicle.

4.1 Kinematic Model of Skid-Steered Mobile Robot

The kinematic equations for the skid-steered mobile robot shown in Fig. 3 are given by

$$\dot{X} = \dot{y}[\cos\Phi + \sin\Phi\tan\alpha] \quad (12)$$

$$\dot{Y} = \dot{y}[\sin\Phi - \cos\Phi\tan\alpha] \quad (13)$$

$$\begin{aligned}\dot{\Phi} &= -\frac{2\dot{y}}{B} + \frac{2r}{B}\omega_o(1-i_o) \\ &= \frac{2\dot{y}}{B} - \frac{2r}{B}\omega_i(1-i_i)\end{aligned} \quad (14)$$

where $[\dot{X}, \dot{Y}, \dot{\Phi}]$ is the velocity vector of the vehicle relative to the global frame, and $\dot{y}$ is given by

$$\dot{y} = \frac{r}{2}\left[\omega_o(1-i_o) + \omega_i(1-i_i)\right] \quad (15)$$

Equations (12), (13) and (14) include the three slip parameters i_o, i_i, α to be estimated by the SMO.

4.2 Sliding Mode Observer for Slip and Velocity Estimation

In (Le 1999), an EKF is used to estimate slip parameters of an excavator based on its kinematic model and simulation results are given. However, the errors in estimated slip parameters increase rapidly as the EKF is a linear estimator used for a nonlinear system. Thus, a nonlinear SMO based on a kinematic model is proposed in this study for slip and velocity estimation (Song, Z. *et al*., 2006). The SMO minimizes the error between the estimated and measured states, converging the estimated states to the real ones, and then the slip and velocity can be estimated.

The observer takes the form of

$$\dot{\hat{X}} = \dot{y}\cos\Phi + L_1 sign(X - \hat{X}) \quad (16)$$

$$\dot{\hat{\Phi}} = -\frac{2\dot{y}}{B} + L_2 sign(\Phi - \hat{\Phi}) \quad (17)$$

$$\dot{\hat{\Phi}}_1 = \frac{2\dot{y}}{B} + L_3 sign(\Phi - \hat{\Phi}_1) \quad (18)$$

where L_1 , L_2 and L_3 are the sliding mode gains, $\dot{\hat{X}}$ and $\hat{X}$ are the estimated velocity and position of the robot in X direction, $\dot{\hat{\Phi}}$ and $\hat{\Phi}$ are the estimated yaw rate and heading angle of the robot, $\dot{\hat{\Phi}}_1$ and $\hat{\Phi}_1$ are dummy variables used for designing an appropriate sliding surface. The error dynamics of the SMO can be obtained by subtracting (16) from (12), (17) from (14) and (18) from (14)

$$\dot{\tilde{X}} = \dot{y}\sin\Phi\tan\alpha - L_1 sign(X - \hat{X}) \quad (19)$$

$$\dot{\tilde{\Phi}} = \frac{2r}{B}\omega_o(1-i_o) - L_2 sign(\Phi - \hat{\Phi}) \quad (20)$$

$$\dot{\tilde{\Phi}}_1 = -\frac{2r}{B}\omega_i(1-i_i) - L_3 sign(\Phi - \hat{\Phi}_1) \quad (21)$$

The error dynamics of the SMO will converge after a finite time interval, provided that the sliding gains are selected to satisfy the derived stability conditions. In (Song Z. *et al*., 2006), Lyapunov stability theory is used to show that if $L_1 > |\dot{y}\sin\Phi\tan\alpha|, L_2 > \frac{2r}{B}|\omega_o(1-i_o)|, L_3 > \frac{2r}{B}|\omega_i(1-i_i)|$, then the SMO is guaranteed to converge within a finite time interval. In other words, $\dot{\tilde{X}} \approx 0$, $\dot{\tilde{\Phi}} \approx 0$ and $\dot{\tilde{\Phi}}_1 \approx 0$.

Given the angular velocities ω_o and ω_i , the vehicle position X , the longitudinal velocity $\dot{y}$ and sliding gains L_1 , L_2 , L_3 , the slip parameters can be calculated as follows

$$\begin{bmatrix} i_o \\ i_i \\ \alpha \end{bmatrix} = \begin{bmatrix} 1 - (L_2 sign(\Phi - \hat{\Phi})_{eq})\dfrac{B}{2r\omega_o} \\ 1 - (L_3 sign(\Phi - \hat{\Phi}_1)_{eq})\dfrac{B}{-2r\omega_i} \\ \pm\cos^{-1}\sqrt{\dfrac{\dot{y}^2\sin^2\Phi}{(L_1 sign(X - \hat{X})_{eq})^2 + \dot{y}^2\sin^2\Phi}} \end{bmatrix} \quad (22)$$

where $(\cdot)_{eq}$ denotes a low pass filter. Substituting (22) into (14), (15) and using the relationship: $\dot{x} = \dot{y}\tan\alpha$, the estimated velocity vector is given as

$$\begin{bmatrix} \dot{\hat{x}} \\ \dot{\hat{y}} \\ \dot{\hat{\phi}} \end{bmatrix} = \begin{bmatrix} \dfrac{r}{2}(\omega_o(1-i_o) + \omega_i(1-i_i))\tan\alpha \\ \dfrac{r}{2}(\omega_o(1-i_o) + \omega_i(1-i_i)) \\ \dfrac{r}{B}(\omega_o(1-i_o) - \omega_i(1-i_i)) \end{bmatrix} \quad (23)$$

For validating the slip vector and velocity vector estimated by the SMO, the forward kinematics of the mobile robot is used to calculate the pose vector $[\hat{X}, \hat{Y}, \hat{\Phi}]$ using the slip vector $[i_o, i_i, \alpha]$ estimated by the SMO. If the trajectory $[\hat{X}(t), \hat{Y}(t), \hat{\Phi}(t)])$ has good agreement with the real one, it is indirectly proved that the estimated slip vector and velocity vector can be accurate.

5. EXPERIMENTAL RESULTS

5.1 Experimental Setup

A skid-steered mobile robot, PIONEER3-AT, is used to experimentally validate the slip and velocity estimation algorithm. The test bed in Fig. 4 (a), is filled with a variety of terrain and allows the mobile robot to move along an arbitrary trajectory. The two driving wheels are equipped with optical encoders with a sampling frequency of 10 Hz for providing wheel angular velocities. A monocular CMOS camera *Silicon Video® 1281* is fixed on the robot in Fig. 4 (b) as a visual odometry sensor. The camera has a resolution of 640 × 512 pixel^2 with a field of view of 40.4º × 30.8º. A frame rate of 30 fps (frame per second) is set to capture images.

For validating the slip and velocity estimation algorithm, a stand-alone overhead vision system, as shown in Fig. 4 (c), is used to provide real trajectory of the robot (Song Z., *et al*,. 2006). The overhead camera with a resolution of 1280 × 1024 pixel^2 measures the motion of the robot by tracking two white round tags pasted on the top surface of the robot. The overhead camera has a high accuracy of 2×10^{-3} m for position and 7×10^{-3} rad for orientation.

In the experiments, the mobile robot is commanded to follow two different trajectories over coarse and fine sands respectively. The robot is driven at speeds ranging from 0.02 m/s to 0.06 m/s.

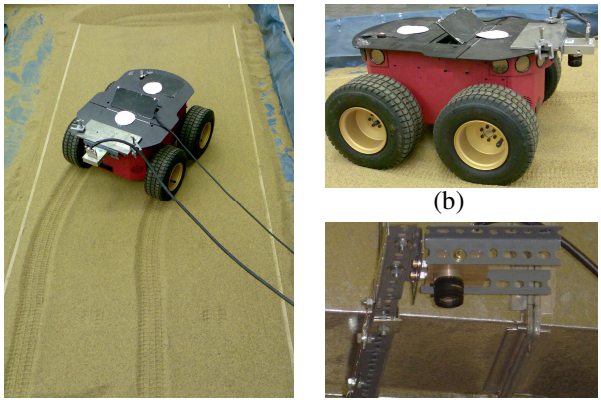

(a) (b) (c)

Fig. 4 (a) Skid-Steered mobile robot in the test bed; (b) On-board camera on mobile robot; (c) Overhead vision system.

5.2 *Experimental Results on Coarse Sand*

Due to the limitation of the test bed, the mobile robot traverses over coarse sand (Garside 60 Sand) along a straight line for 0.19m and then turns along an arc for 0.54m before coming to a halt. Based on the information provided by the visual odometry sensor and the optical encoders, the SMO is driven to estimate the slip vector and velocity vector of the mobile robot. The estimated slip vector and velocity vector in this test are shown in Figs. 5 and 6 respectively.

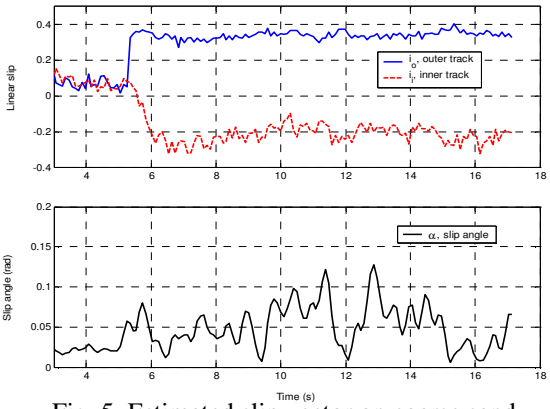

Fig. 5. Estimated slip vector on coarse sand

The mean linear slip of the outer wheel is 34.00% while the mean linear slip of the inner wheel is -21.00%, and the slip angle variably oscillates around 0.05 rad.

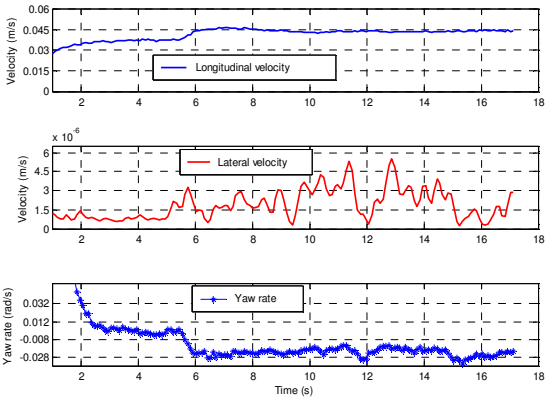

Fig. 6. Estimated velocity vector on coarse sand

The estimated trajectory using the estimate slip parameters from the SMO is compared to the real trajectory constructed from the overhead vision system. In Fig. 7, the trajectory calculated from the forward kinematic equations by using estimated slips are plotted and labelled as *Estimated trajectory*, and the *Trajectory benchmark* is provided by the overhead camera. It is seen the estimated trajectory has good agreement with the benchmark.

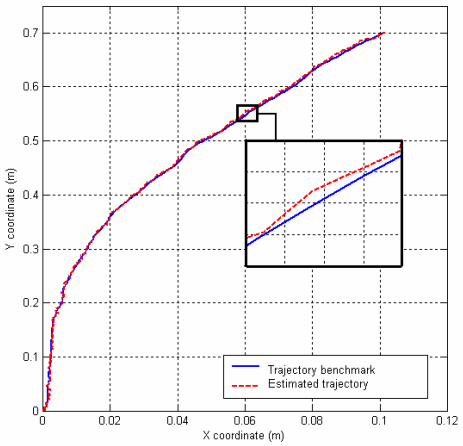

Fig. 7. Estimated trajectory vs. real trajectory

The estimated trajectory has accumulative errors due to once integration and the accumulative trajectory error in this test is 3×10^{-3} m over the range of 0.73 m, less than 1% of the total traveled distance. Comparing the trajectory calculated by the slip and velocity estimation algorithm to the one provided by the overhead camera, we can assure that the slip parameters and velocities estimated by the algorithm are accurate. Additionally, although the estimated trajectory is prone to accumulative errors because of once integration, the estimated slips and velocities are not involved with accumulative errors.

5.3 *Experimental Results on Fine Sand*

In this test, the coarse sand in the test bed is replaced by fine sand (Garside 14/25 Sand). The mobile robot moves along an arc for 0.65 m. Similar with the experiment carried on the coarse sand, the SMO estimates the slip vector and velocity vector of the mobile robot by using the pose and longitudinal velocity information from the visual odometry sensor and wheel angular velocities from the optical encoders. The estimated slip vector and velocity vector are shown in Figs. 8 and 9 respectively.

The forward kinematics of the robot is used to generate the trajectory of the mobile robot using the estimated slip vectors, which are plotted in Fig. 8. As shown in Fig. 10, it is seen that the estimated trajectory has good agreement with the real one provided by the overhead camera. The total accumulative trajectory error is 4×10^{-3} m over the range of 0.65 m, less than 1% of the total traveled distance. Therefore, it can be concluded that the estimated slip and velocity vector by the technique are accurate.

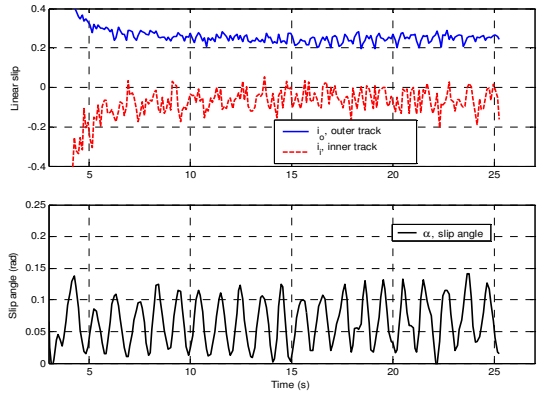

Fig. 8. Estimated slip vector on fine sand

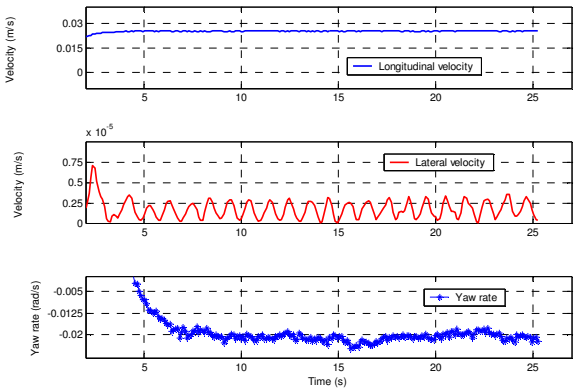

Fig. 9. Estimated velocity vector on fine sand

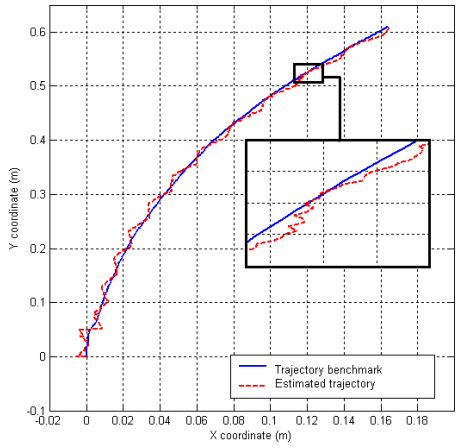

Fig. 10. Estimated trajectory vs. real trajectory

6. CONCLUSIONS

In this paper, we propose a novel vision-based technique for slip and velocity estimation of an UGV. A visual odometry sensor is used to measure the motion of the UGV and provide the inputs for a SMO. The SMO, based-on a kinematic model of the vehicle, is designed to cope with measurement noise and uncertainty and estimate slip and velocity vectors. This slip and velocity estimation technique has been validated on a skid-steered mobile robot over variable terrains with different trajectories. The experimental results show that the technique delivers good performance in slip and velocity estimation when the vehicle moves over terrain at low speeds. Additionally, the estimated slips and velocities are not involved with accumulative errors. Thus, the proposed technique has promising potential applications.

More complex trajectories and longer traveled distance will be attempted in the future work to validate and improve the technique. An IMU is considered to integrate with the visual odometry sensor so that the reliable measured speed ranges of the UGV can be expanded.

REFERENCES

Anderson, R. and D. M Bevly (2004). Estimation of Slip Angles using a Model Based Estimator and GPS. *American Control Conference*, **vol. 3**, pp. 2122-2127.

Barshan, B., H. F. Durrant-Whyte (1995). Inertial Navigation Systems for Mobile Robots. *IEEE Trans. Robotics and Automation*, **vol. 11**, **no. 3**, pp. 328-342.

Bouguet, J-Y. (2007). Camera calibration toolbox for Matlab. [Online].Available:http://www.vision.caltech.edu/bouguetj/calib_doc.

Bunschoten, R. and B. Krose (2003). Visual Odometry from an Omnidirectional Vision System. *IEEE Int. Conf. Robotics and Automation*. **vol. 1**, pp. 577-583.

Cooper, S., H. F. Durrant-Whyte (1994). A Kalman Filter Model for GPS Navigation of Land Vehicles. *IEEE Int. Conf. Intelligent Robots and Systems*, **vol. 1**, pp. 157-163.

Giachetti, A., M. Campani and V. Torre (1998). The Use of Optical Flow for Road Navigation. *IEEE Trans. Robotics and Automation*. **vol. 14**, pp. 34-48.

Le, A.T. (1999). Modelling and Control of Tracked Vehicles. *PhD Thesis*, University of Sydney.

Lee, C., K. Hedrick and K. Yi (2004). Real-Time Slip-Based Estimation of Maximum Tire-Road Friction Coefficient. *IEEE/ASME Trans. Mechatronics*, **vol. 9**, **no.** 2, pp. 454-458.

Lucas, B.D. and T. Kanade (1981). An Iterative Image Registration Technique with an Application to Stereo Vision. *Image Understanding Workshop*, pp. 121-130.

Milella, A., G. Reina and R. Siegwart (2006). Computer Vision Methods for Improved Mobile Robot Estimation in Challenging Terrains. *Journal of Multimedia*. **vol. 1**, **no. 7**, pp. 49-61.

Nagatani, K., S. Tachibana, M. Sofne and Y. Tanaka (2000). Improvement of Odometry for Omnidirectional Vehicle using Optical Flow Information. *IEEE Int. Conf. Intelligent Robots and Systems*. **vol. 1**, pp. 468-473.

Schonemann, P.H. and R. M. Carroll (1970). Fitting One Matrix to Another under Choice of a Central Dilation and a Rigid Motion. *Psychometrika*, **vol. 35**, pp. 245-255.

Shi, J., C. Tomasi (1994). Good Features to Track. *IEEE Int. Conf. Computer Vision and Pattern Recognition*. pp. 593-600.

Song X., L. D. Seneviratne, K. Althoefer, Z. Song and Y. H. Zweiri (2007). Visual Odometry for Velocity Estimation of UGVs. *IEEE Int. Conf. Mechatronics and Automation*, pp. 1611-1616.

Song, Z., Y. H. Zweiri, L. D. Seneviratne and K. Althoefer (2006). Non-linear Observer for Slip Estimation of Skid-Steering Vehicles. *IEEE Int. Conf. Robotics and Automation*, pp. 1499-1504.